In Vivo Three-Dimensional High-Resolution Imaging of Rodent Retina with Spectral-Domain Optical Coherence Tomography

Marco Ruggeri, Hassan Wehbe, Shuliang Jiao, Giovanni Gregori, Maria E. Jockovich, Abigail Hackam, Yuanli Duan, and Carmen A. Puliafito

Purpose. To demonstrate the application of high-resolution spectral-domain optical coherence tomography (SD-OCT) for three-dimensional (3D) retinal imaging of small animals and quantitative retinal information extraction using 3D segmentation of the OCT images.

Methods. A high-resolution SD-OCT system was built for in vivo imaging of rodent retina. OCT fundus images similar to those acquired with a scanning laser ophthalmoscope (SLO) were constructed from the measured OCT data, which provided precise spatial registration of the OCT cross-sectional images on the fundus. A 3D segmentation algorithm was developed for calculation of the retinal thickness map. OCT images were compared by histologic examination.

Results. High-quality OCT images of the retinas of mice (B6/SJLF2 for normal retina, rhodopsin-deficient $Rho^{-/-}$ for photoreceptor degeneration, and $LH_{BETA}T_{AG}$ for retinoblastoma) and rat (Wistar) were acquired. The OCT images compared well with histology. Not only was a 3D image of the tumor in a retinoblastoma mouse model successfully imaged in vivo but the tumor volume was extracted from the 3D image. Retinal thickness maps were calculated that enabled successful quantitative comparison of the retinal thickness distribution between the normal (202.3 ± 9.3 μm) and the degenerative (102.7 ± 12.6 μm) mouse retina.

Conclusions. High-resolution spectral-domain OCT provides unprecedented high-quality 2D and 3D in vivo visualization of retinal structures of mouse and rat models of retinal diseases. With the capability of 3D quantitative information extraction and precise spatial registration, the OCT system made possible longitudinal study of ocular diseases that has been impossible to conduct. (*Invest Ophthalmol Vis Sci.* 2007;48:1808–1814) DOI:10.1167/iovs.06-0815

Rodent models play an irreplaceable role in the study of genetics and the development of new medicine for ocular diseases such as age-related macular degeneration (AMD), glaucoma, and retinoblastoma. AMD and glaucoma are major blinding diseases worldwide. Retinoblastoma is the most common ocular malignancy in children and the third most common cancer to affect children. Researchers using rodent models for AMD[1,2] and glaucoma[3,4] have already provided valuable insight into the genetics and mechanisms of the diseases. It is anticipated that a vast number of studies on the rodent visual system are emerging with the rapid developments of new genetic, biochemical, and physiological tools.[5] Accurate in vivo evaluation of the structural and morphologic changes of the retina is essential for understanding the disease mechanisms and for monitoring disease onset, progression, and response to therapies, which are the keys for developing new treatment strategies and medicine. Retinal morphology and anatomy of small animals can only undergo histologic examination quantitatively after the animals are killed. As a result, a large number of animals must be used to obtain a statistically significant experimental result,[6] and each animal contributes to just a single time point for the full disease progression. It should be emphasized that any such study is inherently cross-sectional, and its ability to evaluate disease progression in a given individual is limited. Noninvasive in vivo examination of the rodent retina and optic nerve without euthanatization of the animal is the key to performing longitudinal studies. It will allow the monitoring of disease progression through its entire course in individual animal models and will provide a better understanding of the pathophysiology of many ocular abnormalities.[4,6]

Optical coherence tomography (OCT)[7,8] is a low-coherence, interferometer-based, noninvasive medical imaging modality that can provide noncontact, high-resolution, cross-sectional images of biological tissue. Since it was first reported more than a decade ago, OCT has been used in a variety of medical research and diagnostic applications, the most successful of which was retinal cross-sectional imaging. Commercial OCT is one of the new standards for in vivo noninvasive ophthalmic imaging and is widely used for diagnosis and treatment monitoring of various ocular diseases in humans. Although OCT has also been used to image the retina in small animals, including mice (Hartl I, et al. *IOVS* 2001;42:ARVO Abstract 4252; Ko TH, et al. *IOVS* 2005;46:ARVO E-Abstract 1051; Shah SM, et al. *IOVS* 2004;45:ARVO E-Abstract 2375; Kim K, et al. *IOVS* 2006;47:ARVO E-Abstract 292),[6,9,10] the reported systems have limitations. In some reports, the depth resolution and the image quality of the systems are not good enough to resolve subretinal layers; therefore, the systems are not suitable for the evaluation of detailed retinal abnormalities.[6,9] They are also not suitable for automatic quantitative retinal analyses. In the other reports, OCT image resolution was good, but a microscopic coverslip was used to press on the mouse cornea to cancel the refractive power of the mouse eye for facilitating light delivery to the retina (Hartl I, et al. *IOVS* 2001;42:ARVO Abstract 4252; Ko TH, et al. *IOVS* 2005;46:ARVO E-Abstract 1051; Shah SM, et al. *IOVS* 2004;45:ARVO E-Abstract 2375; Kim K, et al. *IOVS* 2006;47:ARVO E-Abstract 2923).[10] Because a contact method was used, the systems were not suitable for high-throughput routine applications. Despite limitations, these reports have demonstrated the feasibility of OCT imaging in mouse retina and provided some valuable results.

From the Bascom Palmer Eye Institute, University of Miami Miller School of Medicine, Miami, Florida.

Submitted for publication July 16, 2006; revised September 24 and November 10, 2006; accepted January 25, 2007.

Disclosure: **M. Ruggeri**, None; **H. Wehbe**, None; **S. Jiao**, None; **G. Gregori**, None; **M.E. Jockovich**, None; **A. Hackam**, None; **Y. Duan**, None; **C.A. Puliafito**, None

The publication costs of this article were defrayed in part by page charge payment. This article must therefore be marked "*advertisement*" in accordance with 18 U.S.C. §1734 solely to indicate this fact.

Corresponding author: Shuliang Jiao, Bascom Palmer Eye Institute, University of Miami Miller School of Medicine, 1638 N.W. 10th Avenue Miami, FL 33136; sjiao@med.miami.edu.

The biggest challenge of OCT retinal imaging of the mouse eye comes from the small size of the eye and the very small pupil. The small pupil size of the mouse eye makes the alignment for light delivery to the eye formidable. It also limits the amount of light reflected from the retina and thus decreases the signal-to-noise ratio (SNR). In comparison, the rat eye is approximately twice as big as a mouse eye on a linear scale.[11] Therefore, capturing OCT images of the mouse is, relatively speaking, considerably harder than imaging the rat retina.

In this study, we built a high-resolution spectral-domain OCT (SD-OCT) system for in vivo 3D imaging of the rodent retina. We describe here the test results on B6/SJLF2 (normal retina), $Rho^{-/-}$ (model for photoreceptor degeneration), and $LH_{BETA}T_{AG}$ (model for retinoblastoma) mice and Wistar rat. A 3D segmentation algorithm was applied to the acquired OCT images for the calculation of the retinal thickness map, whereas manual segmentation of the tumor in the retinoblastoma mouse model was made to calculate the tumor volume.

Materials and Methods

Animals

All experiments were performed in compliance with the ARVO Statement for the Use of Animals in Ophthalmic and Vision Research and with the guidelines of the University of Miami Institutional Animal Care and Use Committee. We used 2-month-old B6/SJLF2 mice and 2-month-old Wistar rats, both of which have normal retinas, to assess the imaging capability of the OCT system in rodent retinal imaging. We also examined 4-month-old rhodopsin knockout ($Rho^{-/-}$) mice with photoreceptor degeneration and 9-week-old $LH_{BETA}T_{AG}$ transgenic mouse models of retinoblastoma to demonstrate the capability of the system in imaging the structural changes and tumor in rodent retina. The $Rho^{-/-}$ mouse model, obtained from Dr. Peter Humphries,[12] has a progressive retinal degeneration caused by targeted disruption of both copies of the rhodopsin gene. The $LH_{BETA}T_{AG}$ transgenic mouse model is maintained as a colony in our institution and has been characterized previously.[13] B6/SJLF2 mice are a hybrid of C57BL/6 mice, which have normal retina morphology, and were obtained from Jackson Laboratories (Bar Harbor, ME).

Animals were anesthetized 10 minutes before the experiments by intramuscular injection of a cocktail containing ketamine (80 mg/kg body weight) and xylazine (10 mg/kg body weight). In the meantime, the pupils were dilated with 10% phenylephrine solution. Drops of artificial tears were applied to the animal eyes every 2 minutes to prevent cornea dehydration and cataract formation. Humane killing was performed with CO_2 fumes.

Experimental OCT System

The configuration of the OCT system was similar to what has been reported before except for some specific parameters.[14] A two-module superluminescent diode (SLD) light source (D830-HP2; Superlumdiodes Ltd., Moscow, Russia) with a center wavelength of 830 nm and a full width at half maximum (FWHM) bandwidth of 70 nm was used. The light source provided the low coherence light at a power of 12 mW exiting the single-mode optical fiber pigtail. After passing through a fiber pig-tailed isolator, the low-coherence light was coupled into the source arm of a fiber-based Michelson interferometer that consists of a 2×2 3dB fiber coupler, which split the source light into the sample and the reference arms. The sample arm was interfaced to the modified optical head of an imaging system (OCT 2; Carl Zeiss Meditec Inc., Dublin, CA), which consisted of an X-Y transverse galvanometer scanner and the optics for delivering the sample light to the rodent retina and collecting the back-reflected sample light. A double-aspheric 90-D Volk lens (Volk Optical Inc., Mentor, OH) was used as the objective lens. The power of the sample light was decreased to 750 μW by adjusting the source power with a fiber-based pigtail style attenuator to ensure that the light intensity delivered to the eye was within the ANSI standard and the light exposure was safe for the retina.

In the detection arm, a spectrometer consisting of a collimating lens (f = 50 mm), a 1200 line/mm transmission grating, an achromatic imaging lens (f = 200 mm), and a line scan charge-coupled device camera (Aviiva-M2-CL-2014, 2048 pixels with 14-μm pixel size operating in 12-bit mode; Atmel Corp., Grenoble, France) was used to detect the combined reference and sample light. The calculated spectral resolution was 0.051 nm, which corresponds to a detectable depth range of 3.3 mm in air.[15] An image acquisition board acquired the image captured by the camera and transferred it to a computer workstation (IntelliStation Z Pro, dual 3.6 GHz processor, 3 GB memory; IBM, Armonk, NY) for signal processing and image display. A complete raster scan consisting of 65,536 scanning steps took approximately 2.7 seconds when the A-line (depth scan) rate of the OCT system was set at 24 kHz. At this operating condition, the measured sensitivity was approximately 95 dB. The calibrated depth resolution of the system was approximately 6 μm in the air and approximately 4.4 μm in the tissue (the refractive index of the retina was approximately 1.35).

The challenges for imaging the mouse retina are the very small pupil size and the high dioptric power of the mouse eye. According to Remtulla et al.[11] and Schmucker et al.,[16] the maximum diameter of the pupil of the mouse eye is approximately 2 mm. Through extrapolation from the published data by Remtulla et al.,[11] in which the dioptric power was measured for the wavelength range from 450 nm to 655 nm, the dioptric power at a wavelength of 830 nm (the center wavelength of the OCT system) was estimated to be approximately 550 D. This parameter was used in calculating the scanning range of the OCT image. A six-axis animal mount and alignment system was built for the restraint and adjustment of the animals. We used two mounting tubes of different sizes with fixing holes to restrain mouse and rat, respectively. The fundus camera in the optical head provided initial alignment for the sample light to ensure the sample light was delivered through the dilated pupil. Final alignment was guided by monitoring and optimizing the real-time OCT image of the retina.

OCT Imaging and Histology

We performed experiments on mice and rats. After anesthetization, the animal was restrained in the mounting tube, which was fixed on the six-axis platform. Raster scans—typically we used 512×128 (horizontal $\times$ vertical) and 1024×64 depth scan patterns—with the fast scan in the horizontal direction were performed for each eye. Scan length was approximately 32° for imaging the retinas of mice and rats. With the initial guidance of the fundus camera, experiments showed that the alignment for acquiring a high-quality OCT image took approximately 5 minutes for each mouse eye if the reference arm was tuned correctly. In addition to the cross-sectional images, an en face fundus image similar to the image acquired with a scanning laser ophthalmoscope (SLO) could be generated from the OCT data set.[14]

After imaging, the animals were humanely killed, and both eyes were enucleated and immediately immersion-fixed in 10% formalin for $LH_{BETA}T_{AG}$ and 4% paraformaldehyde, followed by incubation in increasing sucrose concentrations (5%–20%) for $Rho^{-/-}$. $LH_{BETA}T_{AG}$ eyes were embedded in paraffin, sectioned serially in 5-μm sections, and processed for standard hematoxylin-eosin (H&E) analysis. $Rho^{-/-}$ mouse eyes were embedded in embedding media (Tissue Tek; Miles, Elkhart, IN) and flash frozen, and 10-μm serial sections were obtained. Microscopic images of sections were obtained with a digital camera at a magnification of 400×.

Results

OCT Imaging of Normal Rodent Retina

We first describe images of the B6/SJLF2 mouse retina. Figure 1 shows a magnified cross-sectional image from the acquired 3D OCT data set. The OCT image is displayed in grayscale, with darker readings corresponding to lower backscattering and

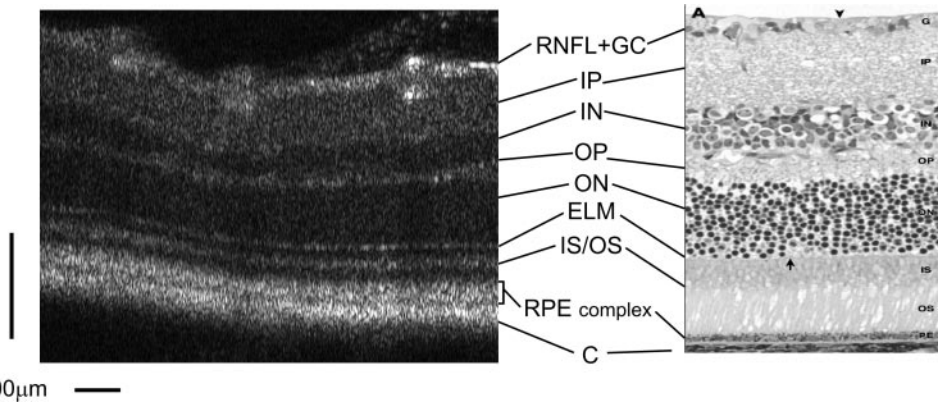

FIGURE 1. Comparison of the OCT cross-sectional image with a textbook histologic image of C57BL/6 mouse retina. All intraretinal layers can be recognized in the OCT image. RNFL, retinal nerve fiber layer; GC, ganglion cell layer; IP, inner plexiform layer; IN, inner nuclear layer; OP, outer plexiform layer; ON, outer nuclear layer; ELM, external limiting membrane; IS/OS, junction between the inner and outer segment of the photoreceptors; RPE complex, retinal pigment epithelium complex; C, choroid. Displayed dynamic range of the OCT image is 35 dB. *Right*: Copyright 2002 from *Systematic Evaluation of the Mouse Eye: Anatomy, Pathology, and Biomethods*, Smith RS, John SWM, Nishina PM, Sundberg JP, eds. Reproduced by permission of Routledge/Taylor & Francis Group, LLC.

brighter regions representing higher backscattering. The image consists of 1024 A-lines covering a range of 1 mm on the retina. All the anatomic layers of the mouse retina can be recognized in the OCT image. For comparison, a published image of a histologic section of a C57BL/6 mouse retina[17] is also shown. The OCT image of the mouse retina is qualitatively similar to that of the human retina: layers consisting of nerve fibers or plexiform layers are optically backscattereding, whereas nuclear layers are weakly backscattering.[18] The OCT image delineated the inner retinal border (inner limiting membrane [ILM]) between the nonreflective vitreous and the backscattering retina. The retinal nerve fiber layer (RNFL) and the ganglion cell layer (GC) represent the first layer in the OCT image, with relatively high backscattering, and can be distinguished as a bright band at the top of the OCT image. Further down in the retina, bands of relatively high and low backscattering can be seen that correspond to the inner plexiform layer (IP), the inner nuclear layer (IN), the outer plexiform layer (OP), and the outer nuclear layer (ON), respectively. The external limiting membrane (ELM), site of numerous occluding junctions, can be visualized. Also shown in the image is the junction between the inner segment (IS) and the outer segment (OS) of the photoreceptors. Beyond the photoreceptor layers a band of high backscattering matches the retinal pigment epithelium complex (RPE complex) that separates the retina from the choroid. We call the region the RPE complex because the band may contain multiple layers, as in the human OCT image. Distal to the RPE complex, the bright high-scattering region is attributable to the choroid (C).

Figure 2 shows the OCT fundus image generated from the measured raw spectral data,[14] together with two cross-sectional images at two different locations for the retina shown in Figure 1. The 3D OCT scan consists of 1024 × 64 (horizontal × vertical) A-lines covering an area of 1 × 1 mm^2 on the mouse retina. The displayed depth of the OCT images is 0.62 mm after correction by the refractive index of 1.35 mm for the mouse retina. The spatial location of each cross-sectional image is marked on the OCT fundus image as a bright line. Features such as blood vessel pattern on the OCT fundus image can be used to achieve good spatial registration for the OCT data set. Spatial registration of the OCT image makes it possible to correlate an OCT data set not only with histologic findings at the same location but also with OCT images taken at different times. Registration of images taken at different times for the same eye during the course of studies is important for research on disease progression and response to therapies by using single animals.

The OCT image crossing the optic disk (Fig. 2C) shows that the nerve fiber layer thickens toward the optic nerve head. As the nerve fiber layer approached the optic nerve head, all the retinal layers became thinner before they terminated. We can also observe the progressive tapering of the retinal layers toward the optic nerve head.

One major difference between the anatomy of the mouse and that of the human is the protruding hyaloid artery remnant (HA),[17] as shown in the OCT image across the optic disk. Even though there is a gradual disappearance of the hyaloid artery with growth, a residue on the surface of the optic nerve head could remain even in adult mice.[17]

Figure 3 shows two cross-sectional images of the retina of a Wistar rat, with one image across the optic disk. With the same scanning angle used for the mouse eye, the 3D image covered an area of 2 × 2 mm^2 on the rat retina. The displayed depth is 0.62 mm, the same as in Figure 2 for the mouse eye. The OCT images consist of 1024 × 64 A-lines.

The OCT data sets not only provided possible 3D visualization of the imaged rodent retina volume and retinal pathologies, they provided comprehensive structural information of the retina. Developing appropriate tools to visualize and quantify the useful structural information from the OCT data sets was a critical step for exploiting the real value of this technology. Several methods are used to display the acquired 3D OCT data. One method is to build the images into a movie and to display the images frame by frame. Another method is to

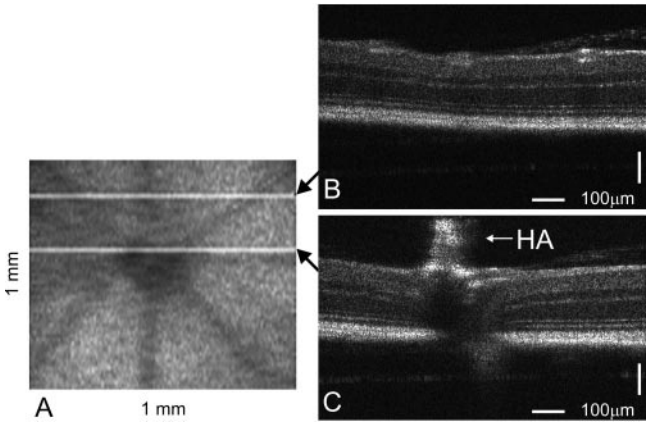

FIGURE 2. The generated OCT fundus image (**A**) of a B6/SJLF2 mouse retina that covers an area of 1 × 1 mm^2 on the retina. Spatial locations of the cross-sectional OCT images distant to the optic disk (**B**) and crossing the optic disk (**C**) are marked on the fundus image with a bright line. HA remnant is shown. Displayed depth of the cross-sectional images is 0.62 mm. Displayed dynamic range of the OCT images is 35 dB.

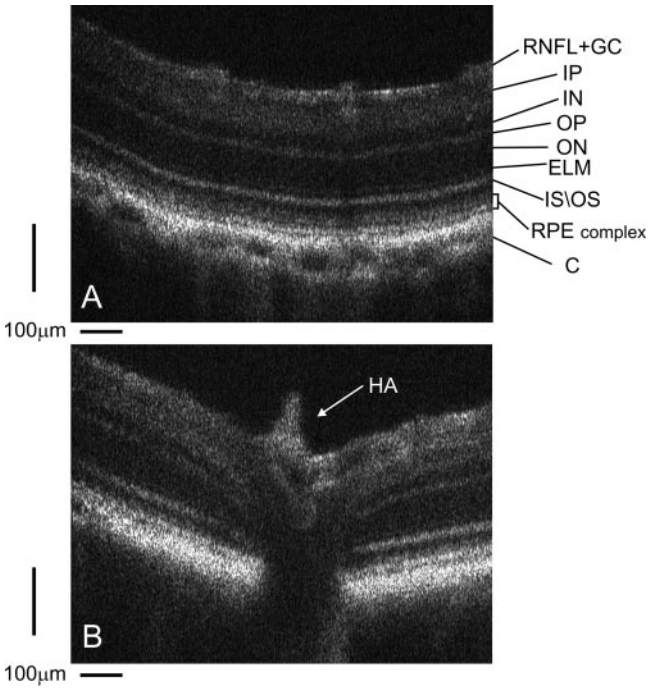

FIGURE 3. Cross-sectional OCT images of a Wistar rat retina distal to (**A**) and crossing (**B**) the optic disk. All the intraretinal layers can be recognized in the OCT images. Displayed dynamic range of the OCT images is 35 dB.

render the 3D data into a virtual 3D image and to provide direct visualization of the whole data set. Figure 4 shows an example of the 3D rendering of the volume OCT data for the B6/SJLF2 mouse retina using commercial software (Amira 4.1; Mercury Computer Systems, Inc., Chelmsford, MA). With this method, the retinal structures could be visualized with cuttings at any position, in any direction, and from any view angle.

OCT Imaging of Degenerative Mouse Retina

One of the main applications of small animal high-resolution OCT is studying the morphologic and structural changes and monitoring these changes over time in animal models of retinal degeneration. To demonstrate the performance of the technology in detecting differences in rodent intraretinal structures, we show here the measured images of mice with photoreceptor degeneration caused by knockout of the rhodopsin gene ($Rho^{-/-}$). Histologic images were obtained for comparison with OCT images of the same mouse eyes. The histologic image (Fig. 5) shows the $Rho^{-/-}$ mouse retina at 4 months of age. Histologic examination of the C57BL/6J retina indicated that for the degenerative retina, the IS and OS layers of the photoreceptors degenerated and outer nuclear (ON) and outer plexiform (OP) layer thickness were significantly reduced. At this age, the inner retinal layers did not show substantial architectural changes; in fact retinal nerve fiber layer (RNFL), ganglion cell layer (GC), inner plexiform layer (IP), and inner nuclear layer (IN) can be recognized in the OCT image (Fig. 5). One prominent feature in the cross-sectional image of the degenerative mouse retina is the much higher signal from the RPE. We believe this is caused by the thinning of the retina—hence, the reduced scattering from the parts in front of the RPE, allowing more light to penetrate the retina and reach the deeper regions. The degenerated outer nuclear layer, the IS, and the OS of the photoreceptors are absent in this OCT image because of severe degeneration of the mouse retina.

OCT Imaging of the Retina of Retinoblastoma Mouse Model

Retinoblastoma is a rare form of cancer that affects the light-sensitive retinal cells that enable sight. Although the disease is rare, it is the most common ocular malignancy in children and occurs in 1 of 15,000 births.[19,20] In the United States, 250 to 350 new cases are diagnosed each year, 90% of which occur in children younger than 5 years of age. When left untreated, this cancer has been uniformly fatal. In the past century, significant advances in screening and treatment have led to virtually all children being cured of the primary eye cancer. Nevertheless, serious concerns exist regarding the significant morbidity and the potential mortality associated with current therapies; therefore, new therapeutic modalities are under investigation. Unfortunately, no technology is available that can provide in vivo quantitative 3D information and precise spatial registration for longitudinal studies.

To assess the capability of the OCT system in imaging retinal tumors, we tested the system on an $LH_{BETA}T_{AG}$ transgenic mouse model of retinoblastoma. In these mice, tumors appear at 4 weeks of age and fill the available orbit volume by 16 weeks of age.[13] Raster scan patterns consisting of 512 × 128 depth scans corresponding to a 1 × 1 mm^2 area on the retina was used for the imaging. Both eyes of 9-week-old $LH_{BETA}T_{AG}$ have been imaged with the OCT system. Histologic images were obtained for comparison with OCT images. The histologic image depicted in Figure 6A shows that the tumor (RT) is in the retinal inner nuclear layer as reported.[13] Figure 6B shows an OCT cross-sectional image of the mouse retina. The tumor can be recognized in the OCT image as a high backscattering region, and the location is in the inner nuclear layer, which is shown more clearly in the 3D display (see Fig. 8).

Quantitative Analysis of the OCT Images

Displaying retinal structures and abnormalities is only the first step for ophthalmic OCT applications. Quantitative evaluation of the damage caused by different diseases to the retina is the key for monitoring disease progression and treatment effect. Therefore, automatic quantitative information extraction from the volume OCT data is one important component for small animal ophthalmic OCT. One important parameter in evaluating damage to the retina is retinal thickness, which was defined as the distance from the ILM to the RPE.

We are developing algorithms for 3D segmentation of various retinal structures, particularly ILM and RPE, from the OCT images. Successful segmentation of such boundaries provides information about the actual geometry of the retina in three dimensions and could generate multiple quantitative parameters (e.g., thickness, curvature, feature sizes) of potential value.

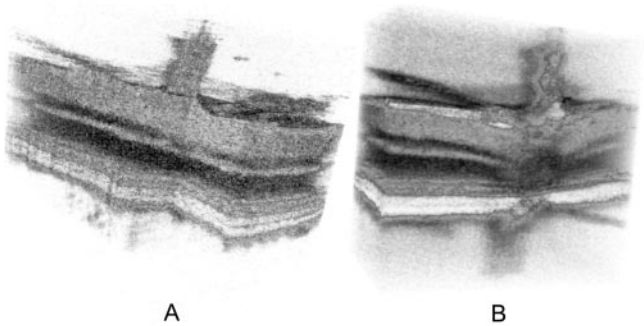

FIGURE 4. Three-dimensional rendering of the B6/SJLF2 mouse retina with different cutting plane and view angle.

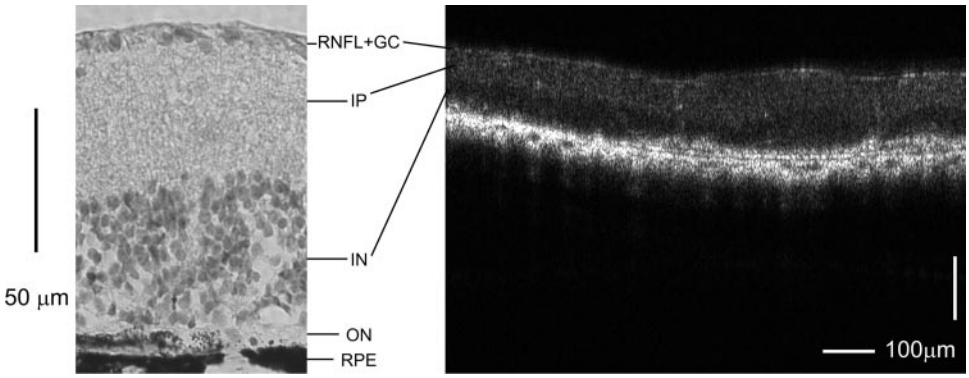

FIGURE 5. Comparison between the histologic image of a $Rho^{-/-}$ retinal degeneration mouse and the cross-sectional OCT image. Displayed dynamic range of the OCT image is 35 dB.

As an illustration of what can be achieved, we present in Figure 7 the output of a preliminary version of the segmentation tools. The algorithm detects the ILM and RPE boundaries by means of an iterative procedure by which an initial guess is repeatedly evaluated and improved. The retinal thickness map can then be easily calculated from the 2D surfaces.

Figure 7 shows the 3D view of the segmented ILM and RPE (Figs. 7A, 7C) and the calculated retinal thickness maps (Figs. 7B, 7D) for B6/SJLF2 and the degenerative ($Rho^{-/-}$) mice, respectively.

To calculate the mean value and the SD of the retinal thickness in the imaged retina area, we averaged all the data points of the thickness map after removing a circular area with a diameter equal to 500 μm around the optic nerve head. The calculated retina thickness for the normal B6/SJLF2 mouse retina was 202.3 $\pm$ 9.3 μm, which was consistent with the thickness previously measured close to the optic nerve head in the C57BL/6 mouse retina.[16] The retinal thickness of the $Rho^{-/-}$ mouse retina was 102.7 $\pm$ 12.6 μm, which matched the retinal thickness measured from fixed sections of the same mouse.

One other significant parameter in evaluating the progression of the disease in retinoblastoma mouse models is the volume of the tumor mass. We calculated the tumor volume with the voxel count method applied to the segmented OCT images acquired on the $LH_{BETA}T_{AG}$ mouse model. The tumor was segmented by manually tracing its boundaries on each cross-sectional OCT image. Figure 8 shows a 3D view of the OCT images; tumor boundaries are highlighted. The 3D image covered a retinal volume of 1 $\times$ 1 $\times$ 0.62 (horizontal $\times$ vertical $\times$ depth) mm^3 consisting of 512 $\times$ 128 $\times$ 1024 voxels, where the imaging depth was corrected by the refractive index of the mouse retina. We then calculated the volume for each voxel of the image as 9.24 μm^3. By counting the total number of voxels confined by the manually segmented boundaries, which was performed automatically by the software, the total volume of the tumor was calculated. The total voxel number occupied by the tumor was 538,165, which yielded a volume of 0.004973 mm^3.

DISCUSSION

Eye movement caused by breathing is obvious in the anesthetized mouse during OCT imaging; it causes oscillating movements of the OCT images primarily in the depth direction. The movement of the OCT images has little effect on the calculation of the retinal thickness map and the generated OCT fundus image. However, it causes distortions to the 3D views of the image and the segmented boundaries. Although the effect can be compensated for during postprocessing, additional restraint for the mouse head is necessary to reduce the effect. We did not compensate eye movement in the present study.

Cornea transparency is one of the keys affecting the quality of the OCT image. Cataract formation in the eye of rodents under anesthesia is a limiting factor for OCT imaging. To keep the eye transparent, examination time should be as short as possible, and artificial tears should be applied to the cornea regularly. Imaging of the conscious rodent is more reliable if the animal is suitably restrained.

Results presented in this study demonstrated the capability of our OCT system to image retinal structures in normal and diseased rodent eyes. The acquired OCT images have excellent correlation with histology. The reported OCT system accomplished the goal of noninvasive noncontact in vivo imaging of the rodent retina with high image quality and short examination time (approximately 5 minutes; image acquisition time, 2.7 seconds), making the system suitable for routine high throughput repeatable applications. The acquired volume data

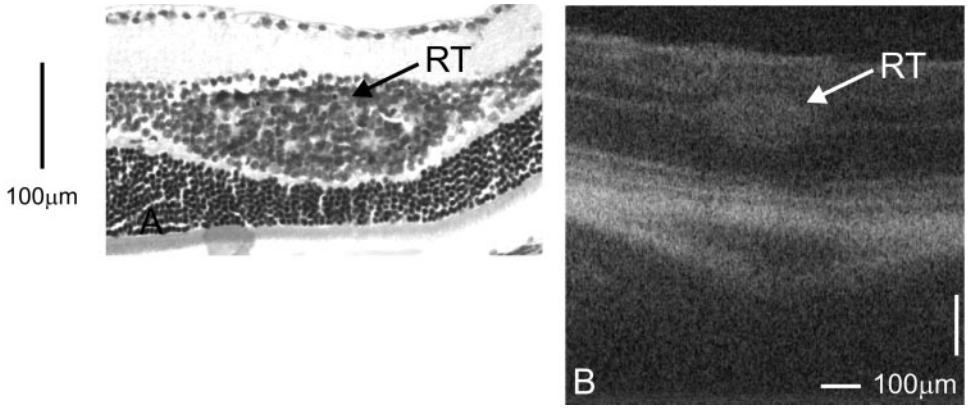

FIGURE 6. (**A**) Histologic image of the retinal tumor (RT) in the inner nuclear layer of an $LH_{BETA}T_{AG}$ transgenic mouse retina. (**B**) Cross-sectional OCT image crossing the tumor. Displayed dynamic range of the OCT image is 35 dB.

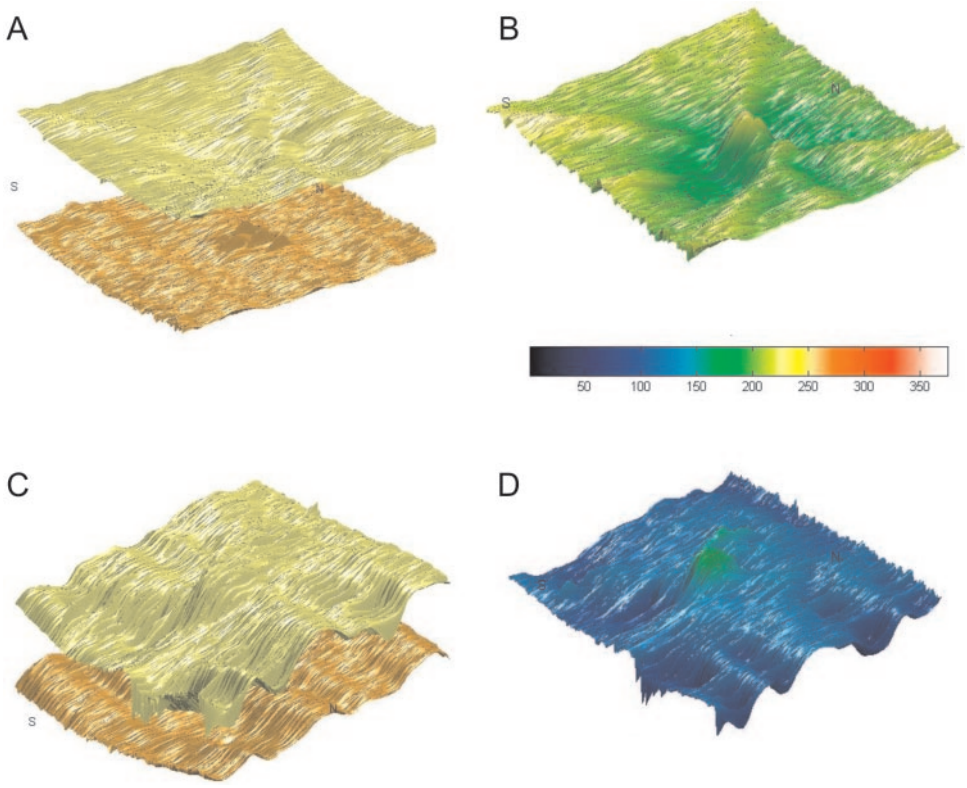

FIGURE 7. (**A**) Three-dimensional segmentation of the ILM and RPE for the normal B6/SJLF2 mouse retina. (**B**) Retinal thickness map of normal mouse retina. (**C**) Three-dimensional segmentation of the ILM and RPE for the Rho$^{-/-}$ mouse retina. (**D**) Retinal thickness map of the Rho$^{-/-}$ mouse retina. Color map range is from 0 μm to 375 μm. Calculated average retinal thicknesses are 202.3 $\pm$ 9.3 μm for the B6/SJLF2 mouse and 102.7 $\pm$ 12.6 μm for the Rho$^{-/-}$ mouse, respectively.

not only provide 3D views of the retina and retinal abnormalities, they also provide means for precise comparison of the images acquired at different time points, making longitudinal study of retinal diseases in rodent models possible. The OCT fundus image provides a tool for precise spatial registration of the OCT cross-sectional images on the retina and potentially for precise registration of the OCT images with histologic sections.

Three-dimensional automatic segmentation allows quantitative evaluation of the morphology and structure of different retinal layers. The current segmentation algorithm developed by our group can successfully extract the ILM and the RPE and, in turn, provide the thickness map of the rodent retina. Segmentation of the tumor boundary (manual in the present study) allowed calculation of the tumor volume that would allow monitoring the response to therapies. Algorithms for automatic or semiautomatic segmentation of the boundaries among different retinal layers and other retinal features (i.e., retinal tumors) are under development.

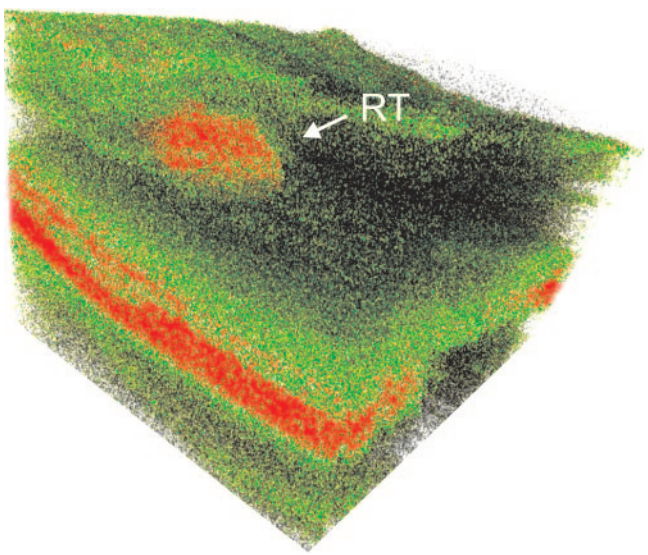

FIGURE 8. Three-dimensional rendering of the OCT images with highlighted tumor boundaries of an $LH_{BETA}T_{AG}$ transgenic mouse retina.

Acknowledgments

The authors thank Xiangrun Huang, Jie Ouyang, Fabrice Manns, Omer Kocaoglu, Vittorio Porciatti (all from Bascom Palmer Eye Institute) and Weizhao Zhao (Department of Biomedical Engineering, University of Miami) for their support of the experiments.

References

1. Ambati J, Ambati BK, Yoo SH, Ianchulev S, Adamis AP. An animal model of age-related macular degeneration in senescent Ccl-2- or Ccr-2-deficient mice. *Nat Med*. 2003;9:1390–1397.
2. Karan G, Lillo C, Yang Z, et al. Lipofuscin accumulation, abnormal electrophysiology, and photoreceptor degeneration in mutant *ELOVL4*transgenic mice: amodel for macular degeneration. *Proc Natl Acad Sci USA*. 2005;102:4164–4169.
3. Levkovitch-Verbin H, Quigley HA, Martin KRG, Valenta D, Baumrind LA, Pease ME. Translimbal laser photocoagulation to the trabescular meshwork as a model of glaucoma in rats. *Invest Ophthalmol Vis Sci*. 2002;43:402–410.
4. Grozdanic SD, Kwon YH, Sakaguchi DS, Kardon RH, Sonea IM. Functional evaluation of retina and optic nerve in the rat model of chronic ocular hypertension. *Exp Eye Res*. 2004;79:75–83.
5. Wu SM, Baehr W, Crair M. The mouse visual system: from photoreceptors to cortes. *Vis Res*. 2004;44:3233–3234.
6. Li Q, Timmers AM, Hunter K, et al. Noninvasive imaging by optical coherence tomography to monitor retinal degeneration in the mouse. *Invest Ophthalmol Vis Sci*. 2001;42:2981–2989.
7. Huang D, Swanson EA, Lin CP, et al. Optical coherence tomography. *Science*. 1991;254:1178–1181.

8. Fercher AF, Hitzenberger CK, Kamp G, El-Zaiat SY. Measurement of intraocular distances by backscattering spectral interferometry. *Opt Commun*. 1995;117:43–48.
9. Horio N, Kachi S, Hori K, et al. Progressive change of optical coherence tomography scans in retinal degeneration slow mice. *Arch Ophthalmol*. 2001;119:1329–1332.
10. Srinivasan VJ, Wojtkowski M, Fujimoto JG, Duker JS. In vivo measurement of retinal physiology with high-speed ultra-high-resolution optical coherence tomography. *Opt Lett*. 2006;15: 2308–2310.
11. Remtulla S, Hallett PE. A schematic eye for the mouse, and comparisons with the rat. *Vis Res*. 1985;25:21–31.
12. Humphries MM, Rancourt D, Farrar GJ, et al. Retinopathy induced in mice by targeted disruption of the rhodopsin gene. *Nat Genet*. 1997;15:216–219.
13. Windle JJ, Albert DM, O'Brien JM, et al. Retinoblastoma in transgenic mice. *Nature*. 1990;343:665–669.
14. Jiao S, Knighton R, Huang X, Gregori G, Puliafito C. Simultaneous acquisition of sectional and fundus ophthalmic images with spectral-domain optical coherence tomography. *Opt Express*. 2005;13: 444–452.
15. Häusler G, Lindner MS. Coherence radar and spectral radar—new tools for dermatological diagnosis. *J Biomedical Opt*. 1998;3:21–31.
16. Schmucker C, Schaeffel F. A paraxial schematic eye model for the growing C57BL/6 mouse. *Vis Res*. 2004;44:1857–1867.
17. Smith RS, John SWM, Nishina PM, Sundberg JP. *Systematic Evaluation of the Mouse Eye: Anatomy, Pathology and Biomethods*. Boca Raton, FL: CRC Press; 2002.
18. Drexler W, Morgner U, Ghanta RK, Kärtner FX, Schuman JS, Fujimoto JG. Ultra-high-resolution ophthalmic optical coherence tomography. *Nat Med*. 2001;7:502–507.
19. Tamboli A, Podgor MJ, Horm JW. The incidence of retinoblastoma in the United States: 1974 through 1985. *Arch Ophtalmol*. 1990; 108:128–132.
20. Pendergrass TW, Davis S. Incidence of retinoblastoma in the United States. *Arch Ophthalmol*. 1980;98:1204–1210.